G. Pitarresi et alii, Frattura ed Integrità Strutturale, 30 (2014) 127-137; DOI: 10.3221/IGF-ESIS.30.17

Focussed on: Fracture and Structural Integrity related Issues

Photoelastic stress analysis assisted evaluation of fracture toughness in hydrothermally aged epoxies

G. Pitarresi, A. Toscano, M. Scafidi, M. Di Filippo, S. Alessi, G. Spadaro

University of Palermo, Dipartimento di Ingegneria Chimica, Gestionale, Informatica, Meccanica (DICGIM) – Viale delle Scienze, 90128 Palermo (Italy)

giuseppe.pitarresi@unipa.it, andrea.toscano@unipa.it, michele.scafidi@unipa.it, maria.difilippo@unipa.it, sabina.alessi@unipa.it, giuseppe.spadaro@unipa.it

ABSTRACT. The present work has investigated the fracture toughness of a model DGEBA epoxy system subject to Hidro-Thermal aging. A Photoelastic Stress Analysis technique has been implemented, showing the evolution of stresses arising throughout the water uptake process due to the non-uniform swelling of the material. Gravimetric and Dynamic Mechanical Thermal Analyses have further complemented the characterization, showing the onset of plasticization effects with aging. The correlation of all previous characterizations has allowed to conclude that an increase of K_{IC} fracture toughness is obtained at the fully saturated condition. In particular Photoelasticity has also revealed the onset of relevant swelling induced stresses during the first stages of water absorption, leading to an increase of fracture toughness due to compressive stresses settling near the crack tip. A stress free condition is instead reestablished at the later stages of absorption, suggesting that the increased toughness of the saturated material is an effect of the modifications induced by aging on the polymer structure.

KEYWORDS. Fracture Toughness; Hydrothermal Aging; Thermosetting Resin; Swelling Stresses; Photoelastic Stress Analysis.

INTRODUCTION

Glossy polymer structures, such as thermoset matrices used in Fiber Reinforced Plastic (FRP) composites, are in general prone to solvents absorption. A more or less severe solvent exposure depends on the working conditions, and in general both civil or transport applications may present very aggressive environments, which can activate various aging phenomena in the material. Water uptake by exposure to wet environments is in particular a most studied aging condition for thermoset resins [1-3]. In fact a vast literature is now available which has investigated the kinetics of water diffusion, and the physical and chemical transformations occurring in the material [4]. The nature of such transformations is rather variegate. The absorbed water is for instance differentiated into free and bonded water [1,4-7], with the bonded water chemically reacting with sites of the polymer chain, e.g. by means of hydrolysis. Such chemical interactions can modify the network structure, increasing the molecular chain mobility (plasticization), and also modifying the free volume, which in turns can interfere with the amount of absorbed free water. Another consequence of such diffusion-reaction changing scenario is the swelling deformation of the network [7,8], which can have important mechanical consequences, especially when the polymer is somewhat constrained to other more inert materials [7].

Hygroscopic swelling can indeed give rise to important internal stresses when materials interfaces are present, e.g. matrix/fibre, adhesive bonding, electronic packaging, etc.
In order to simulate the long-term consequences of water uptake, accelerated aging is usually implemented by increasing the temperature of the conditioning environment, usually consisting of a water bath (hydro-thermal aging) or a controlled humid airborne climate chamber (hygro-thermal aging) [9,10]. The material is then monitored at specific stages by applying a number of physical characterizations, the most common of which are Gravimetric analyses and Dynamic Mechanical Thermal (DMTA) analyses [4]. Based on this approach, several studies are available who have focused on the interactions between the diffusion kinetics and the polymer network structure [1-10].
Some important aspects of the mechanical behavior of aged glassy polymers have though received relatively little attention so far, and in particular the evaluation of the residual internal stresses and strains induced by swelling, and the consequences of the polymer network modifications on the polymer fracture toughness.
Regarding the first aspect, only a few experimental approaches have been proposed to determine swelling induced strains, and to quantify the swelling sensitivity of the polymer. An average strain can be measured by a Thermal Mechanical Analyzer (TMA) [11], and then correlated to water concentration to evaluate the Coefficient of Hygroscopic Swelling. This technique though does not take into account the transient non-uniform strain distribution in the sample. Full filed optical techniques such as Moirè Interferometry [7,12] or Digital Image Correlation [13-16] have been also implemented, being able to measure full field in-plain strains simultaneously to water diffusion. Both techniques though require staring at the sample constantly, and are then rather complicate to implement with hydrothermal conditioning. Furthermore, they require some degree of sample surface preparation.
Regarding the second aspect of fracture toughness modifications, it is observed that water uptake usually produces a decrease of the Glass Transition temperature, T_g, well detected by the DMTA [4,9]. Such increased polymer chain mobility is usually interpreted as a plasticization effect, and as such, it should produce an increase of fracture toughness. A direct verification of this correlation is though rarely found in the literature [9], although fracture toughness parameters for brittle plastics are well characterized by the theory [17], and measurable with standardized procedures [18,19]. Water uptake may also induce some generalized degradation effects in the material, which can counterbalance the plasticization. An example of such unpredictable behavior is the lack of a well established trend about the influence of water uptake on Mode I delamination toughness of FRPs [20]. The literature survey in [20] has also evidenced how most of work on delamination of aged FRPs do not investigate the modifications of fracture toughness in the resin matrix in bulk conditions.
The present work implements a Photoelastic Stress Analysis (PSA) technique that is able to measure the evolution of stresses during water diffusion in epoxy materials [21]. Some unique features of the proposed approach include the possibility to directly measure stresses with a very high sensitivity, the fast acquisition of full-field non-contact measurements, and the use of a simple optical setup and low cost equipment [22]. The only restricting requirement is the need for transparency and optical birefringence of the material being tested.
PSA is in particular used in this work to investigate the stress field arising in hydrothermally aging cracked samples. These consist of Single Edge Notched Bending (SENB), prepared according to ASTM D5045 [18] for the evaluation of fracture toughness. The material investigated is a model epoxy system, prepared by mixing a DGEBA monomer with an amine DDS curing agent, and cured with an optimized thermal cycle, able to determine a high T_g (> 200 °C) and a fully cured and stress free state. The SENB samples have been aged by resting in a water bath at 80 °C, up to a fully saturated condition, achieved after about 1300 hours. A number of characterizations have been performed throughout the aging conditioning, comprising: Gravimetric Analysis, DMTA, PSA and Fracture Toughness tests. PSA in particular was carried out by placing the beam samples into a circular polariscope at regular intervals during aging. Isochromatic maps were acquired in both white and monochromatic light, and a quantitative analysis was carried out by implementing a Tardy Phase-Shifting Method (TPSM) [23].
The extensive characterization has allowed to conclude that the epoxy system increases its intrinsic fracture toughness K_{IC} of about 39% at the fully saturated condition. At the early stages of water absorption the swelling stresses are particularly severe and determine an increase of fracture toughness that is due to compressive stresses settling near the crack tip.

MATERIALS AND METHODS

The DGEBA-DDS epoxy analyzed in this work can be considered as a model system due to its widespread consideration in the literature. This base epoxy system is in fact present in many commercial matrix formulations adopted in the composites industry, in particular for the making of high T_g matrices and pre-impregnated laminas.

All tested samples in this work have been in-house prepared by cast molding. The following subsections describe the preparation and physical-mechanical characterization of the samples in more details.

Preparation of samples and plan of experiments

The resin system was prepared by mixing a monomer base: 2,2-bis[4-(glycidyloxy)phenyl]propane (DGEBA) and a 4,4' diamino-diphenyl sulfone (DDS) curing agent. A stoichiometric amount of DDS was fully dissolved into the DGEBA monomer by mechanical stirring for 30 minutes at 130°C.

The resin blend was cast into a rectangular mould surface (250×250 mm^2) made of a polished steel, previously treated with a Marbocote TRE45ECO release agent. The mould was laterally bounded by depositing two beads of acetic silicone. This allowed the curing at high temperature and easy release of the cast resin plate, which also presented a clear and uniform transparency, fundamental for the implementation of transmission Photoelasticity.

An optimized curing cycle was applied consisting of a permanence at 180 °C for 2 hours, cooling to room temperature and post-curing by resting at 200°C for 2 hours, followed by a slow cooling to room temperature in 24 hours. Between the curing and post-curing stages, the resin plate was cut into small rectangular samples of nominal dimensions of 30×8×3 mm^3. These dimensions in particular were compliant with the SENB samples in ASTM D5045 [18], and with the requirements for the DMTA tests. The post-curing cycle was performed on the un-cracked rectangular beams, and was able to completely relieve any initial residual stresses from the material.

All the implemented characterizations have been performed on the above mentioned rectangular beams, which were all cut from the same manufactured panel.

Tab. 1 summarizes the tests performed and the number of samples tested.

Characterization	Number of Samples			Testing Condition			Type of Sample
Gravimetric	3			entire aging cycle			un-cracked
DMTA	(2)	(2)	(2)	(PC)	(48h)	(S)	un-cracked
PSA	2			entire aging cycle			un-cracked
PSA	2			entire aging cycle			SENB
Fracture Toughness	(5)	(5)	(5)	(PC)	(48h)	(S)	SENB

Table 1: Characterization methods and relative number and type of tested samples. PSA stays for Photoelastic Stress Analysis, and indicates the acquisition of three images (see the subparagraph on PSA). PC stays for postcured (not aged), 48h stays for aged in the thermal bath for 48 hours, and S stays for saturated.

Hydrothermal conditioning

Aging conditioning of the samples consisted in their immersion in a bath of deionized water, kept at constant 80 °C. The samples were taken out of the conditioning environment at regular times to perform the gravimetric and photoelastic (non-destructive) tests, and the DMTA and fracture toughness (destructive) tests. The time needed to weigh the samples and to acquire the photoelastic images was of the order of few minutes. This short interval time did not affect the absorption kinetic and stress state of the samples.

Gravimetric and Dynamic Mechanical Thermal Analyses

Samples were weighed on a 0,01 mg resolution electronic balance. The sample surface was gently wiped out of superficial water before weighing. Weight measurements have been taken throughout absorption up to 1320 hours. Results are presented in terms of relative mass change versus the square root of time, t, with the relative mass change defined by:

$$\text{relative mass change}: \frac{W_t - W_i}{W_i} \times 100 \tag{1}$$

where w is the weight and the subscript i indicates the initial weight and t the actual weight.

The Dynamic Mechanical Thermal Analysis (DMTA) was performed on a Rheometric Scientific DMTA V, in a single cantilever beam arrangement at a heating rate of 10°C/min. The tanδ versus temperature curve is in particular considered, with the values of T_g approximated as the temperatures corresponding to peaks.

Fracture Toughness

All samples for the Mode I fracture toughness evaluation have been prepared in accordance with ASTM D5045 [18]. The Single Edge Notched Bending configuration has been chosen in particular. The introduction of the edge crack was obtained in two steps: a first notched slot was machined by means of a small table band saw, with a thin blade of thickness 0.3 mm (14 teeth per inch). The length of this first notch is usually slightly smaller than half the sample height, $B/2$. Razor tapping on a razor blade hold in place by the thin notch slot, and resting against the notch root has then introduced a sharp crack. A repeated razor tapping, using always a fresh blade at each tap, has been found to be an effective way to introduce and grow a sufficiently long cracked zone. A qualitative criterion used to grow the crack is to make this slightly bigger than the notch slot width (> 0.5 mm). The very good transparency of the material has resulted a very useful feature in order to visually check the introduced crack, and adjust the tapping force to optimize the crack length and crack front straightness. Care was taken to guarantee that the overall crack (notch plus crack) had a length falling between $0.45<a/B<0.55$ (in accordance with the standard).

All SENB tests have been performed on an Electro-Mechanic Instron 3367 testing machine equipped with a 1 kN load cell, and measuring the load *vs* mid-span displacement curve in three point bending. A circular polariscope was fitted in the testing machine in order to acquire photoelastic images of the samples at various stages of the test loading. An RGB JVC ccd camera and a Nikon D5100 camera, with an optical setup optimized for Macro photography, were both used to acquire images of the samples on the polariscope. The Photoelastic images helped also in the correct placement of the SENB sample, using the symmetry of the isochromatic fringes as an index of the correct positioning and centering of samples on the three point bending rig.

The critical stress intensity factor K_{IC} (cSIF) is obtained by the data reduction scheme of ASTM D5045-96 (the latter 1999 version of this standard requires a fixed S/W ratio of 4, not accounting for slight departures). The evaluation of K_{IC} was preferred to that of G_{IC}, which requires the computation of load/displacements areas and the correction for indentation energy, making this parameter more prone to errors. The evaluation of K_{IC} requires only a critical load to be chosen from the acquired test data, according with the formula:

$$\left(K_Q\right)=\left(\frac{P_Q\cdot s}{B\cdot W^{3/2}}\right)\cdot\underbrace{\frac{3}{2}x^{1/2}\frac{\left[1.99-x(1-x)(2.15-3.93x+2.7x^2\right]}{\left(1+2x\right)\left(1-x\right)^{3/2}}}_{f(x)} \tag{2}$$

where K_Q is the provisional cSIF, P_Q is a critical load, B the sample thickness, W the sample height and s the span [18].

It is observed here that the cross-check criterion given in the standard to verify the existence of Plain Strain conditions for the tested specimen geometry, was checked by using literature values of the epoxy yield stress. Even by considering conservative values, the criterion was always widely satisfied, due to the highly brittle behavior of the material.

Photoelastic Stress Analysis

The application of Photoelasticity on the hydrothermally aging epoxy is made possible by the optical property of birefringence exhibited by the material [22]. The smooth surface finish of the mould used to cast the sample panel determined a suitable optical transparency of the cast resin.

Isochromatic maps of samples have in particular ben obtained by transmission Photoelasticity from a circular polariscope in dark or light field, using a white or monochromatic light source (see also Fig. 1).

Due to the geometry and load symmetry of the standard SENB specimen, the principal stress orientation in the points lying on the vertical central section are oriented parallel to the sample edges [21, 23-27]. In light of this, the Tardy Phase-Shifting Method (TPSM) [24] represents a potentially effective quantitative photoelastic technique. This is a simplified phase-shifting method already used for the analysis of the membranal stress distribution of tempered glass plates [23]. The typical set-up of the polariscope used for this technique is shown in Fig. 1.

Depending on the angle β_A of the Analyzer A, the light intensity I emerging from the photoelastic model, C, placed inside the polariscope is:

$$I=I_f+\frac{I_0}{2}\left(1-\cos 2\pi\delta\cos 2\beta_A+\sin 2\pi\delta\sin 2\beta_A\cos 2\alpha\right) \tag{3}$$

where I_f and I_0 are, respectively, the background and the reference intensities, α is the orientation of the bigger principal stress σ_1 and δ is the relative retardation. The quantity of interest is the retardation δ that is related to the principal stress difference by the following relationship:

$$\delta = \frac{Cd}{\lambda}(\sigma_1 - \sigma_2) \tag{4}$$

where C is the Photoelastic constant of the material, d the thickness of the model and λ the wavelength of the light source. The monochromatic light source used for this work is a sodium vapor lamp with a λ=589 nm wavelength.

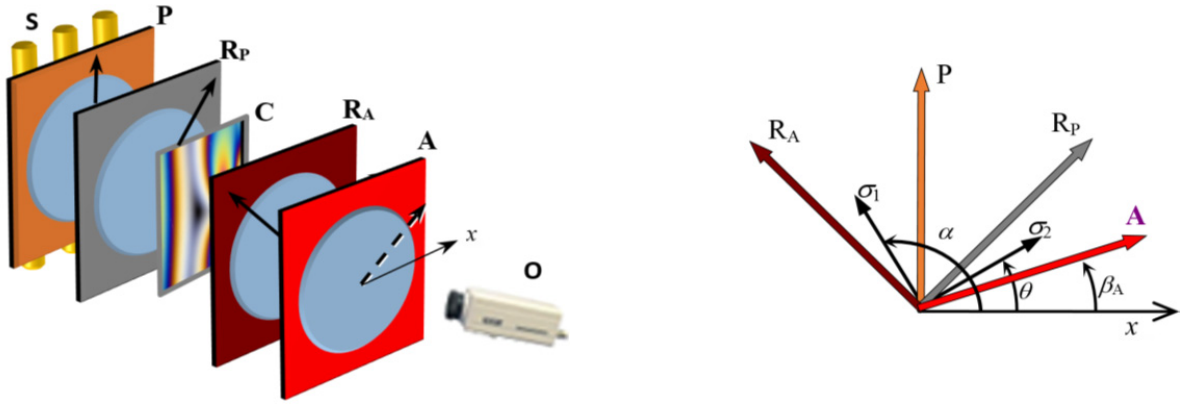

Figure 1: Tardy Phase-Shifting Method: polariscope set-up.

The constant C depends on the photoelastic material analyzed in the experiment, and on the wavelength of the light source. The C constant of the material considered in this work is not known and has to be determined by a direct calibration. Using a four point bending calibration method on a rectangular beam cut form the same casted resin plate of the SENB samples, the measured value is C=6.53×10^{-5} mm^2/N.

A quantitative evaluation of the isochromatic parameter (σ_1-σ_2) is then provided for the points of the vertical symmetry axis laying between the crack tip and the opposite straight edge, aligned with the crack orientation. To perform such evaluation, the TPSM requires the acquisition of three different images to determine δ. These images are acquired by setting the orientation of the analyzer as β_{A1}=0°, β_{A2}=45°, β_{A3}=90°. Considering that the orientation of the principal stresses in the considered section is aligned whit the edge of the model (α=0° or α=90°), the emerging intensities I_i (i=1,2,3) are:

$$I_1 = I_f + \frac{I_0}{2}(1 - \cos 2\pi\delta) \tag{5}$$

$$I_2 = I_f + \frac{I_0}{2}(1 \pm \sin 2\pi\delta) \tag{6}$$

$$I_3 = I_f + \frac{I_0}{2}(1 + \cos 2\pi\delta) \tag{7}$$

where the upper and lower sign in eq. 6 is respectively for α=0° and α=90°.

The retardation δ is determined by combining Eq. (5)-(7) in the next Eq. (8):

$$\delta = \frac{1}{2\pi} arctan \frac{I_1 + I_3 \pm 2I_2}{I_3 - I_1} \tag{8}$$

where the same sign convention of eq. 6 is valid.

RESULTS AND DISCUSSION

The following two subparagraphs present the results of the physical characterization and Photoelastic qualitative and quantitative stress analysis. The third subparagraph presents the results of the fracture toughness tests, correlating them to the whole set of characterization data.

Absorption kinetic and Glass Transition temperature

Fig. 2a shows the measured relative mass change versus the square root of time. Data are averaged from three samples, and standard deviation scatter bands are not shown as they were too narrow. It is noticed that diffusion follows a Fickian behavior [4, 6, 21], with a first linear increase, and the establishment of a saturation plateau at around 3.5% of relative mass uptake. The behavior is also in general well agreement with the findings of other authors on similar materials and conditions [6, 10, 28].

Fig. 2b shows the tanδ versus temperature curve form the DMTA. A sufficient approximation of the value of T_g is given by the temperature at the tanδ peak. With this assumption, the PC samples have a T_g of about 230 °C. Two successive conditions have been characterized, i.e. after 48 hours of immersion in the thermal bath, and at saturation (after 1320 hours). At 48h it is observed that the curve widens towards smaller temperatures, and the tanδ peak has a slight decrease, while the T_g is little modified and there is still a unique well defined peak. These changes indicate that only a small portion of material is undergoing a transformation. At saturation the curve is wider and a double peak is formed. Both peak temperatures are at lower temperature values compared to the original and 48h T_g. Such modifications indicate a less cross-linked network structure and an increased molecular chains mobility, and hence an increased ductility or a plasticization effect.

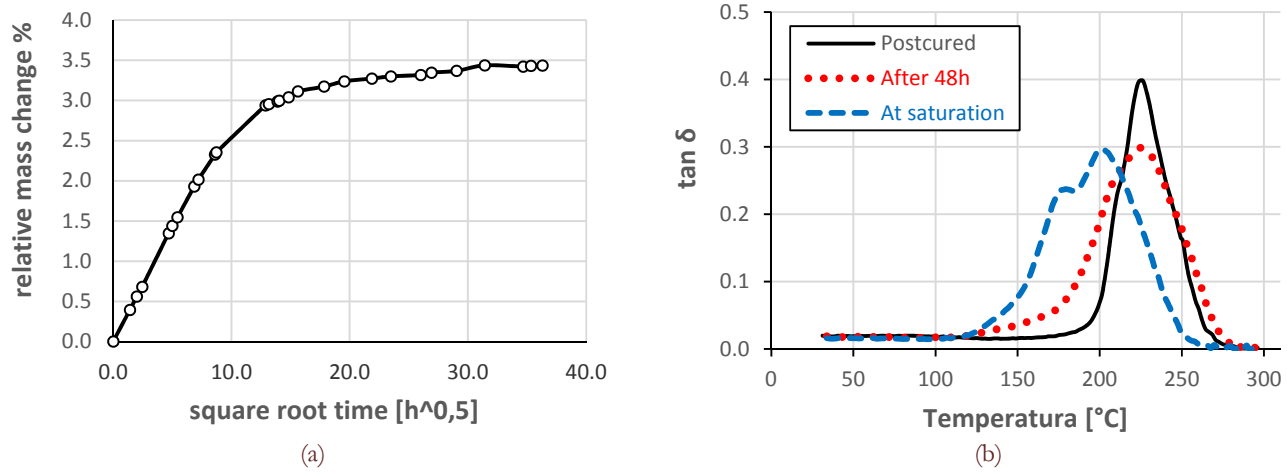

Figure 2: (a) Gravimetric analysis results; (b) DMTA tanδ curves at various aging stages.

Photoelastic analysis of transitory swelling stresses

The different concentration of absorbed water during the first stages of diffusion determines a non-uniform swelling [21]. The mutual constraint between swelled and un-swelled zones induces a peculiar stress field that is well detected by Photoelasticity. In Fig. 3a the isochromatic map is shown, acquired in white light and dark field circular polariscope, for an un-cracked sample taken out of the thermal bath after about 48 hours. It is first of all noticed that the fringes have a symmetric pattern distribution. This means that the swelling deformation of the material, related to water concentration, is also symmetric, and that concentration is increasing regularly in all directions at the same rate. Dark fringes in white light Photoelasticity also indicate the loci with zero fringe order, i.e. where σ_1-σ_2=0.

A quick qualitative interpretation of the observed stress pattern is possible by focusing on the straight and longer border of the sample. Here the main stress component is σ_x (see the reference axes of fig. 3 for a correct interpretation of stress directions), and it is σ_x<0, i.e. compression. This compression arises due to the constraint of the inner material, (un-deformed) towards the outer material which wants to expand (swell).

In Fig. 3b stress profiles are plotted along the central vertical section, obtained with the TPSM data reduction procedure outlined before. Although the analysis provides σ_x-σ_y, being not able to fully separate the stresses, it is observed that σ_y is small and negligible in first approximation. The trends in Fig. 3b can then be more easily interpreted as those of σ_x. In light of this, it is immediate to conclude that the central part of the sample is in prevalent traction (along the beam axis direction x), while the side part is in compression. It is also observed that for equilibrium to be satisfied, the traction and compression zones should have a null force and momentum resultants.

Fig. 4a shows the isochromatic maps acquired at different aging times for a cracked SENB sample. It is noticed that the swelling stresses arise at the very early stages of water ingress. For instance, after 7 hours, the stress distribution is well

formed and the peak stresses are reached at some time between 7 and 48 hours of immersion in the thermal bath. As diffusion proceeds and reaches the inner parts of the material, the swelling stresses start to progressively relax and an almost fully stress free situation is reestablished at saturation.

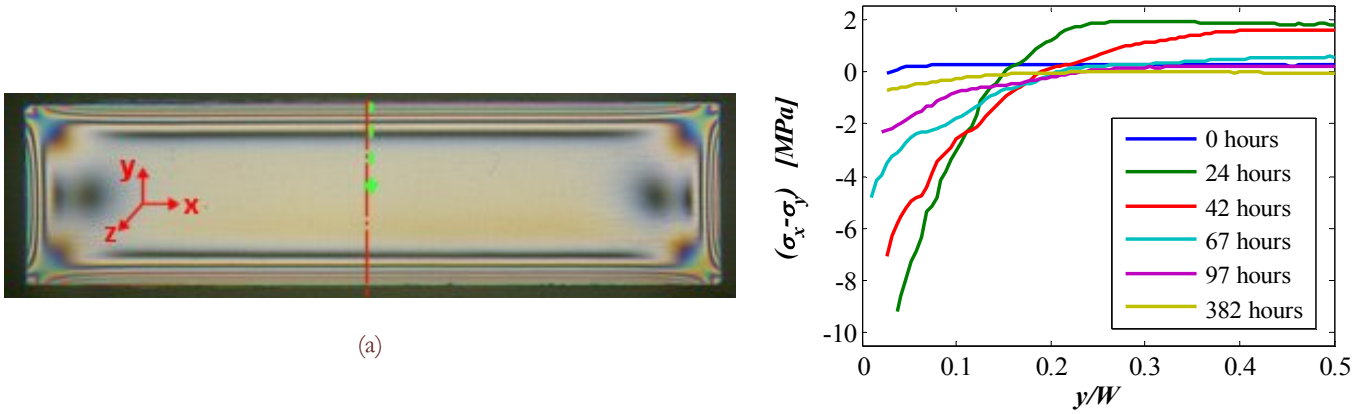

Figure 3: (a) isochromatic map from white light dark field circular polariscope of an un-cracked sample after 48 hours of immersion in the thermal bath; (b) Plot of (σ_x-σ_y) along the vertical axis of symmetry, going from the sample edge to the sample centre (green dashed line), at different aging times.

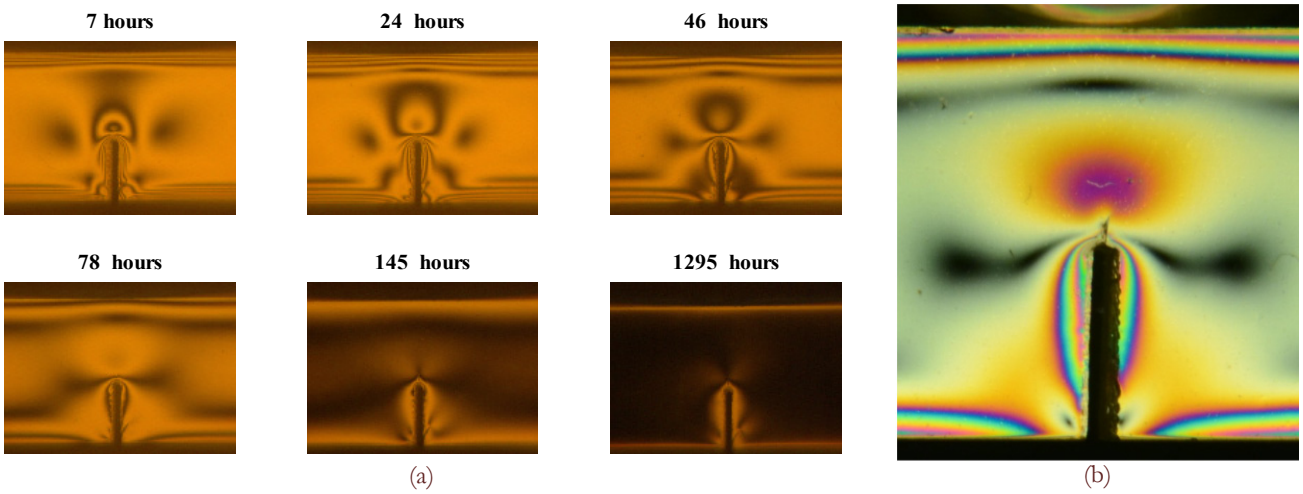

Figure 4: (a) Evolution with aging time of isochromatic maps from SENB samples, acquired with a dark field circular polariscope in monochromatic light; (b) particular of the notched zone, acquired in white light, after 48 hours aging.

From Fig. 4 it is also observed that the presence of the crack does modify significantly the fringe pattern near the crack tip. This changes are mainly induced in order to preserve the self equilibrated nature of the swelling stresses. As seen for the un-cracked sample (Fig. 3), going from side to side along the vertical symmetry axis requires two inversions of the sign of σ_x, from negative to positive to negative again, in order to maintain a null moment resultant. The same trend should settle for the cracked sample, this time considering the ligament of material going form the crack tip to the upper straight border.

Indeed Fig. 4b shows how the black fringe (σ_1-σ_2=0) is formed on the wake of the crack, anticipating a change of sign of σ_x. The flanks of the sharp crack (i.e. that formed by razor tapping) are very likely compressed against each other with a steep rise of the negative σ_x value, in order to preserve equilibrium. On the contrary, in the zones ahead of the crack tip there is an increase of the fringe order due to an increase of the tensile stress component σ_x. This increase is probably due to a combined effect of the compressive crack closure on the wake of the crack, and the singularity of the crack discontinuity.

Fig. 5 shows the results of the TPSM evaluation, providing σ_x-σ_y along the ligament of material ahead of the crack, having length *W-a*. Plots in Fig. 5a are parameterised versus time, and (contrary to the plot in Fig. 3b) the origin of the *y* coordinate is now at the crack tip. Compared to the un-cracked sample, it is seen that the values of σ_x-σ_y are now bigger in the central part of the sample. The curves at 7 hours and 30 hours also reach a maximum value at some distance ahead of the crack tip, and then they start to decrease, indicating the inversion of the trend. Unfortunately, the TPSM is not able to resolve the fringe order, and hence to evaluate stresses, very near the crack tip. Plots in Fig. 5b highlight the evolution of stresses versus time on selected points of the ligament. It is in particular observed how the swelling stresses quickly arise in the first hours from the beginning of diffusion, and after about 200 hours (i.e. about the 8% of the total time to saturation) they are almost completely relieved.

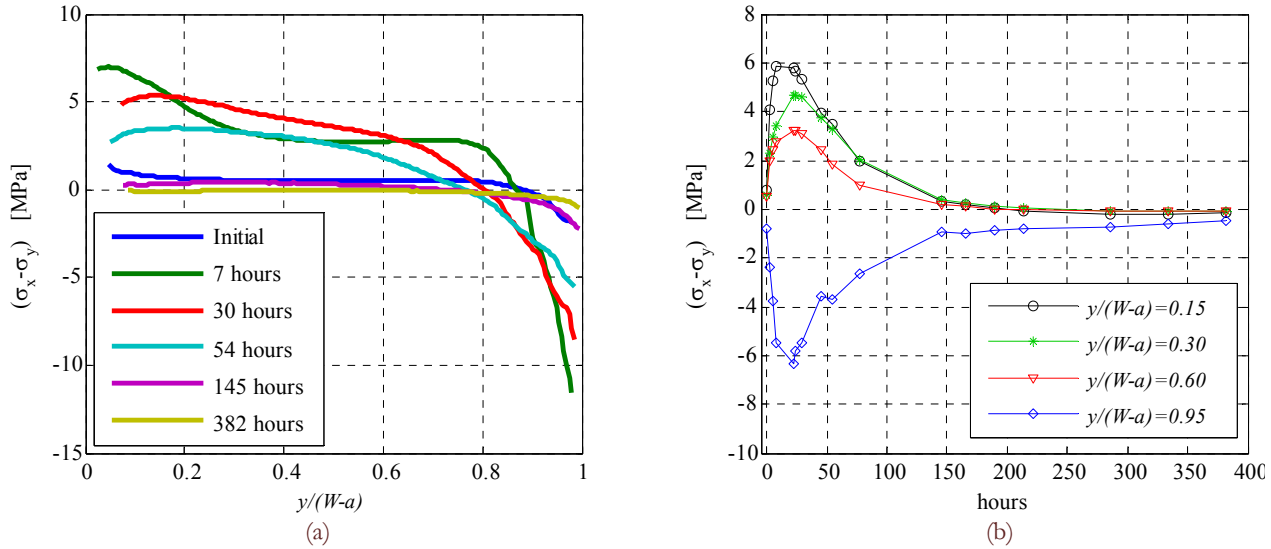

Figure 5: (a) Plots of (σ_x-σ_y) along the ligament of material ahead of the crack, for various aging times; (b) plots of (σ_x-σ_y) versus time on selected points of the same ligament.

Fracture toughness results

Fig. 6a shows three examples of force versus mid span displacement curves, acquired during the three point bending loading of the SENB samples, at the three monitored conditions: postcured, 48 hours aged and saturated. On Fig. 6b the values of the critical SIF K_{IC} are reported. The values are averaged from five tests per condition, and the standard deviation scatter band is also shown.

The fracture toughness of the non-aged material is in agreement with other works from the same authors [9,28], on similar epoxy systems, indicating a good repeatability of the test results. The fracture toughness measured after 48 hours of resting in the thermal bath is sensibly higher, with an increase of about 75%. Since the DMTA test has not evidenced a significant plasticisation effect after 48 hours, it is concluded that such increase is determined by the state of internal stresses induced by the non-uniform swelling. In particular, the increase of toughness is explained with the compressive stresses acting very near the crack tip, and on the wake of the crack, already discussed in the previous sub-paragraph.

The fracture toughness at complete saturation is also showing an increase of about 39% compared to the not-aged material. This is smaller than the increase observed at the 48h condition, but still a meaningful increase. Since the photoelastic technique has revealed that the material is completely free of stresses at this stage of aging, the increase of fracture toughness can be safely attributed to the plasticisation effects brought about by the modifications of the polymer network structure, already confirmed by the DMTA (Fig. 2).

From Fig. 6a it is interesting to observe that the PC samples exhibit a slower crack propagation, witnessed by the many sampled points after the reach of the peak load which activated the crack propagation. The 48h and S samples on the contrary exhibited an instantaneous drop of load due to a fast crack growth. For the 48h samples this is probably due to the traction stresses ahead of the crack which may feed the fracture with further strain energy.

Fig. 7 shows the isochromatic maps of a SENB sample subject to increasing loads during the three point bending fracture test. It is in particular possible to observe how the typical Mode I singular stress field predicted by the Linear Elastic Fracture Mechanics is superimposed to the initial stress distribution produced by the non-uniform swelling. Near the loading nose it is immediate to observe that the photoelastic fringes are attracted towards the nose, and this is typical of a

boundary under compression stresses. As the load increases the points on the vertical symmetry axis (x=0) should produce a black fringe since the Westergaard equations predict that $\sigma_1=\sigma_x=\sigma_2=\sigma_y$ [29]. It is instead observed a more complicate behaviour, due to the traction and compression σ_x stresses already present from the aging process. Further work in the future will try to find a quantitative interpretation of this observed superposition of stress field and its influence on the fracture behaviour of the material.

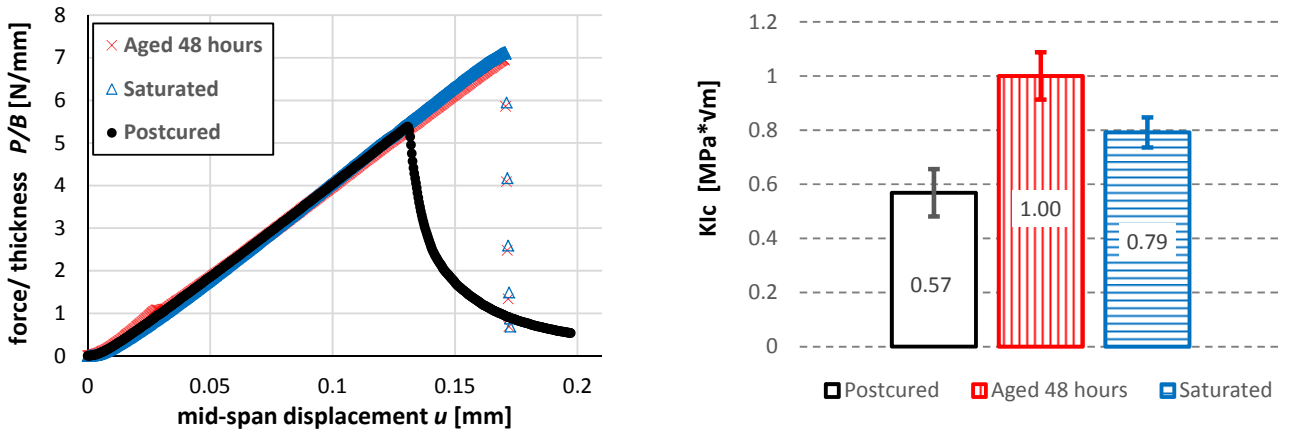

(a) (b)

Figure 6: (a) Plots of normalized force versus displacement from SENB samples; (b) Value of KIC fracture toughness measured at the three monitored conditions.

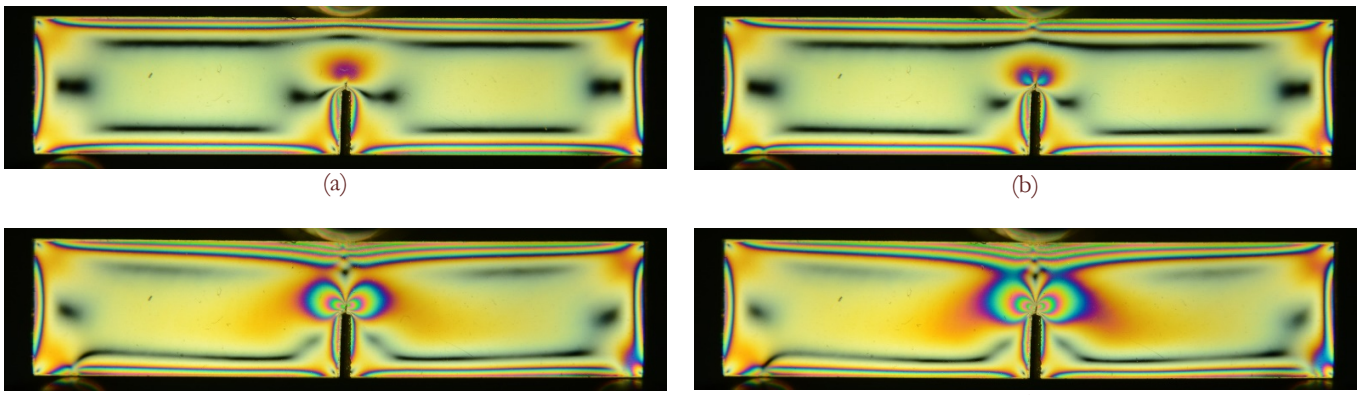

(a) (b)

(c) (d)

Figure 7: Isochromatic maps of SENB sample (circular dark field polariscope in white light) during the three point bending fracture test, at various applied loads: (a) 0 N; (b) 2 N; (c) 8 N; (d) 10 N.

CONCLUSIONS

The present work has proposed an experimental evaluation of the influence of Hydrothermal aging on the fracture toughness of a model DGEBA-DDS epoxy system. The work in particular has successfully implemented a Photoelastic image analysis technique exploiting the optical transparency and birefringence of the epoxy material. Photoelasticity has proved to be a very effective, sensitive and easy to set-up methodology to monitor the stresses arising in the material during the initial stages of water ingress and diffusion. The analysis of the stresses by Photoelasticity, performed throughout the aging period up to complete saturation, has allowed to establish that the stress field is induced by the non-uniform swelling between the inner and outer parts of the sample. The Photoelastic analysis has also evidenced that the presence of a crack, in the Single Edge Notched samples considered in this work, determines a peculiar stress distribution near the crack tip. For the given geometry of the tested samples, the stresses have reached their peak within the first 48 hours of aging, and have then gradually been relieved until the reestablishment of a complete stress free condition at saturation.

The critical Stress Intensity Factor K_{IC} measured at 48 hours aging showed a 75% increase from the reference not-aged condition. Such increase is believed to be due to compressive stresses acting near the crack tip and on the wake of the crack, as evidenced by the qualitative and quantitative analysis of the acquired photoelastic images. The fracture toughness at saturation has shown an increase of about 39% with respect to the not-aged condition. This growth is instead not determined by the swelling stresses. It is then explained as the result of a plasticization of the material, i.e. of the modifications induced by the hydrothermal aging on the polymer network structure, which were also confirmed by the Dynamic Mechanical Thermal Analysis performed in this work.

REFERENCES

[1] Zhou, J., Lucas, J.P., Hygrothermal effects of epoxy resin. part I: The nature of water in epoxy, Polymer, 40(20) (1999) 5505-5512.

[2] VanLandingham, M.R., Eduljee, R.F., Gillespie Jr, J.W., Moisture diffusion in epoxy systems, J Appl Polym Sci, 71(5) (1999) 787-798.

[3] Nogueira, P., Ramírez, C., Torres, A., Abad, M.J., Cano, J., López, J., López-Bueno, I., Barral, L., Effect of water sorption on the structure and mechanical properties of an epoxy resin system, J Appl Polym Sci, 80(1) (2001) 71-80.

[4] Starkova, O., Buschhorn, S.T., Mannov, E., Schulte, K., Aniskevich, A., Water transport in epoxy/MWCNT composites, European Polymer Journal, 49(8) (2013) 2138-2148.

[5] Apicella, A., Tessieri, R., de Cataldis, C., Sorption modes of water in glassy epoxies. J Membr Sci, 18(C) (1984) 211-25.

[6] Jackson, M., Kaushik, M., Nazarenko, S., Ward, S., Maskell, R., Wiggins, J., Effect of free volume hole-size on fluid ingress of glassy epoxy networks, Polymer, 52(20) (2011) 4528-4535.

[7] Fan, X.J., Lee, S.W.R., Han, Q., Experimental investigations and model study of moisture behaviors in polymeric materials, Microelectronics Reliability, 49(8) (2009) 861-871.

[8] Xiao, G.Z., Shanahan, M.E.R., Swelling of DGEBA/DDA epoxy resin during hygrothermal ageing, Polymer, 39(14) (1998) 3253-3260.

[9] Alessi, S., Conduruta, D., Pitarresi, G., Dispenza, C., Spadaro, G., Accelerated ageing due to moisture absorption of thermally cured epoxy resin/polyethersulphone blends, thermal, mechanical and morphological behavior, Polym Degrad Stab, 96(4) (2011) 642-648.

[10] Li, L., Yu, Y., Wu, Q., Zhan, G., Li, S., Effect of chemical structure on the water sorption of amine-cured epoxy resins, Corros Sci, 51(12) (2009) 3000-3006.

[11] Zhou, J., Transient analysis on hygroscopic swelling characterization using sequentially coupled moisture diffusion and hygroscopic stress modeling method, Microelectronics Reliability, 48(6) (2008) 805-810.

[12] Stellrecht, E., Han, B., Pecht, M.G., Characterization of hygroscopic swelling behavior of mold compounds and plastic packages, IEEE Transactions on Components and Packaging Technologies, 27(3) (2004) 499-506.

[13] Jackson, M.B., Heinz, S.R., Wiggins, J.S., Fluid ingress strain analysis of glassy polymer networks using digital image correlation, Polym Test, 31(8) (2012) 1131-1139

[14] Park, S., Zhang, H., Zhang, X., Ng, S.L., Lee, H.C., Temperature dependency of coefficient of hygroscopic swelling of molding compound, Proceedings - Electronic Components and Technology Conference, art. no. 5074012 , (2009) 172-179.

[15] Jang, C., Yoon, S., Han, B., Measurement of the hygroscopic swelling coefficient of thin film polymers used in semiconductor packaging, IEEE Transactions on Components and Packaging Technologies, 33(2) (2010) 340-346.

[16] Madduri, S., Infantolino, W., Sammakia, B.G., An experimental and computational study on moisture induced epoxy swelling in nonhermetic optoelectronic packages, J Electron Packag, Trans ASME, 134(1) (2012).

[17] Moore, D.R., Pavan, A., Williams, J.G., Fracture testing method for polymer, adhesives and composites, ESIS Publication No. 28, Elsevier (2001).

[18] ASTM D 5045-96, Standard test methods for plane-strain fracture toughness and strain energy release rate of plastic materials, (1996).

[19] ISO 13586, Plastics -- Determination of fracture toughness (GIC and KIC) -- Linear elastic fracture mechanics (LEFM) approach, (2000).

[20] Alessi, S., Pitarresi, G., Spadaro, G., Effect of hydrothermal ageing on the thermal and delamination fracture behaviour of CFRP composites, Composites: Part B, 67 (2014) 145-153.

[21] Pitarresi, G., Scafidi, M., Alessi, S., Di Filippo, M., Billaud, C., Spadaro, G., Water absorption kinetics and swelling stresses in an epoxy resin system studied by means of Photoelastic image analyses, submitted to Polymer Degradation and Stability (August 2014).
[22] Ramesh, K., Photoelasticity. In Springer handbook of experimental solid mechanics (Ed. W. N. Sharpe), 2008 701–742 (Springer, New York, New York).
[23] Ajovalasit, A., Petrucci, G., Scafidi, M., Measurement of edge residual stresses in glass by the phase shifting method, Optics and Lasers in Engineering, 49(5) (2011) 652-657.
[24] Ajovalasit, A., Petrucci, G., Scafidi, M., Photoelastic analysis of edge residual stresses in glass by automated "test fringes" methods, Experimental Mechanics, 52(8) (2012) 1057-1066.
[25] Ajovalasit, A., Petrucci, G., Scafidi, M., RGB photoelasticity applied to the analysis of membrane residual stress in glass, Measurement Science and Technology, 23(2) (2012) art.n.025601.
[26] Ajovalasit, A., Petrucci, G., Scafidi, M., Photoelastic analysis of edge residual stresses in glass by the automated tint plate method, Experimental Techniques, doi: 10.1111/ext.12017 (in press) (2013).
[27] Ajovalasit, A., Petrucci, G., Scafidi, M., A critical assessment of automatic photoelastic methods for the analysis of edge residual stresses in glass, The Journal of Stress Analysis for Engineering Design, 49(5) (2014) 361-375.
[28] Pitarresi, G., Alessi, S., Tumino, D., Nowicki, A., Spadaro, G., Interlaminar fracture toughness behavior of electron-beam cured carbon-fiber reinforced epoxy-resin composites, Polymer Composites, 35(8) (2014) 1529-1542.
[29] Janssen, M., Zuidema, J., Wanhill, R. J. H., Fracture Mechanics, Spon Press (2004).